Viscoplastic constitutive equations of combustion chamber materials including cyclic hardening and dynamic strain aging

Jean Louis Chaboche, Anaïs Gaubert, Pascale Kanouté, Arnaud Longuet, Farida Azzouz, Matthieu Mazière

Viscoplastic constitutive equations of combustion chamber materials including cyclic hardening and dynamic strain aging

J.-L. Chaboche [a,*], A. Gaubert [a], P. Kanouté [a], A. Longuet [b], F. Azzouz [c], M. Mazière [c]

[a] *Onera – The French Aerospace Lab, F-92322 Châtillon, France*
[b] *Safran Group, Snecma Villaroche, 77550 Moissy-Cramayel, France*
[c] *Centre des Matériaux – Mines ParisTech, BP 87, F-91003 Evry Cedex, France*

Cobalt-base and nickel-base superalloys for aircraft engine combustion chamber applications (e.g. Haynes 188, Haynes 230, Hastelloy X) show a complex viscoplastic behavior. In a large temperature range from 300 to 800 °C, an important cyclic hardening with memory effects combined with a negative strain rate sensitivity are observed. This behavior can be related to the dynamic strain aging phenomenon. The present contribution aims at proposing a set of constitutive equations that are able to predict those experimental observations. A classical unified viscoplastic framework is coupled with a physically motivated macroscopic modeling of dynamic strain aging initially introduced by McCormick and Kubin, Estrin. The complete model has been identified on original multilevel and multirate cyclic experiments and cyclic relaxation experiments on the Haynes 188 alloy. The predictive abilities of the model are demonstrated by simulations of a large set of experimental data including fatigue tests from the literature.

1. Introduction

Optimization of performances (cost, security) and lifetime assessment of critical parts working under complex cyclic thermomechanical conditions remains a challenging problem for aircraft turbine engines, for which new improvements are still necessary. This is especially true in the context of combustion chambers, transition ducts, and after-burner components, in principle less critical components (because not rotating), as they sustain very high cyclic thermal gradients, which results from start-up and shut-down procedures. A complex series of processes, involving not only fatigue, but also creep, creep-fatigue interaction and crack propagation, could cause the final failure of these high temperature components.

The lifetime analysis needs to first perform the cyclic inelastic analysis, leading to more or less cyclically stable responses, then a damage assessment based on creep, fatigue coupled with environment, estimating both macro-crack initiation and its propagation.

Though many progresses have been done during the past 20 years concerning multiscale approaches of the inelastic analysis of structural components, there is still the need for using more macroscopic approaches of the material constitutive modeling, at the continuum scale of the component.

The context of the present paper concerns the development of cyclic inelastic constitutive equations that are able to capture and to reproduce the main facts observed on materials currently used for combustion chambers, like Co based superalloys Haynes 188, Haynes 230, or Ni based superalloys like Hastelloy X, all of them, surprisingly, showing similar trends in their monotonic as well as cyclic behaviors and their variation with temperature.

* Corresponding author.
E-mail address: chaboche@onera.fr (J.-L. Chaboche).

At room temperature, as well as at high temperature these materials behave like many other alloys, involving a classical strain rate sensitivity (SRS). However, in the intermediate temperature range, from 300 to about 800 °C, they are demonstrating both an extremely pronounced cyclic hardening (with no tendency to saturate even after several thousands of cycles) and a quite significant inverse strain rate sensitivity, associated with dynamic strain aging (DSA). Other effects are also present, like static recovery of kinematic hardening, even at moderate temperatures like 600 °C.

Many experimental results can be found in papers by Miner and Castelli (1992), Rao et al. (1995, 1997), and Chen et al. (2001, 2004), that confirm these trends. On the other side, there exist several constitutive models that have some capabilities to describe coupled effects of cyclic hardening, softening and dynamic strain aging, which will be mentioned in Section 3. However, they do not seem to have been applied on the kind of alloys considered in the present paper, especially when taking into account both the important cyclic hardening and the inverse SRS.

The main objective of the paper is then to propose some modifications and extensions to an existing constitutive framework, in order to offer the capability to describe the main experimental facts observed on these superalloys used in combustion chambers. Section 2 introduces the general structure of the classical cyclic viscoplastic constitutive equations used at Onera (Chaboche, 1989, 2008) and recalls their main capabilities. Various methods that have been used to introduce DSA effects in similar constitutive equations are briefly recalled and discussed in Section 3. The main experimental observations from the literature are recalled and a series of more recent special tests in tension–compression is also presented in Section 4. Moreover, it is shown how the classical model may be modified in order to describe the observed additional effects and couplings. The identification strategy of the constitutive model is also presented. Section 5 gives the main comparisons between the experimental results and the model simulations, for the tests used in the identification step as well as for those which were not used. Some additional tests are then predicted, in particular tests taken from the literature.

2. Classical constitutive framework

The unified structure of the adopted constitutive model consists in using one single mechanism, represented by the plastic (or viscoplastic) strain. All equations are written for isothermal conditions but their generalization under varying temperature is a simple and standard procedure. The thermodynamic consistency of this class of constitutive framework has been established since a long time (see Chaboche (1996) for instance). The specific case studied later in this paper (Section 4.2) will be discussed in Appendix A.

2.1. Flow equations

In the context of small deformations the total strain is partitioned into:

$$\underset{\sim}{\varepsilon} = \underset{\sim}{\varepsilon}^e + \underset{\sim}{\varepsilon}^p \tag{1}$$

Plastic flow is governed by the elasticity domain, defined by $f < 0$ in the stress space, with f expressed as:

$$f = J(\underset{\sim}{\sigma} - \underset{\sim}{\mathbf{X}}) - Y \tag{2}$$

where J defines an invariant function in stress space, for instance von Mises invariant. $\mathbf{X}$ is the back stress tensor and Y defines the current size of the elastic domain, evolving by isotropic hardening. We use the normality assumption, considering the associated plasticity framework:

$$\dot{\underset{\sim}{\varepsilon}}^p = \dot{\lambda}\frac{\partial f}{\partial \underset{\sim}{\sigma}} = \dot{\lambda}\,\underset{\sim}{\mathbf{n}} \tag{3}$$

where $\underset{\sim}{\mathbf{n}}$ represents a unit direction, using the norm in the plastic strain space such that $\frac{2}{3}\,\underset{\sim}{\mathbf{n}} : \underset{\sim}{\mathbf{n}} = 1$. In the case of viscoplasticity f may be positive, and the overstress (or viscous stress) σ_v expresses: $\sigma_v = f = J(\underset{\sim}{\sigma} - \underset{\sim}{\mathbf{X}}) - Y$. The multiplier $\dot{\lambda}$ is then a given function of the overstress (and other variables if needed), not necessarily deriving from a viscoplastic potential (we adopt here the formulation given in Chaboche (1997)). In the present case we choose an hyperbolic sine dependency:

$$\dot{\lambda} = \dot{\varepsilon}_0 \sinh\left(\left\langle\frac{\sigma_v}{K}\right\rangle^n\right) \tag{4}$$

We still use a stress exponent as this function degenerates to Norton's law for the low stresses. Many experimental results show, even for pure metals and at high temperature (Freed and Walker, 1993), that exponents like 3 or 3.5 are still necessary (pure diffusional creep is a very limited case). With von Mises criterion, using $J(\underset{\sim}{\sigma}) = (3/2\,\underset{\sim}{\sigma}' : \underset{\sim}{\sigma}')^{1/2}$, where $\underset{\sim}{\sigma}'$ is the stress deviator, the norm of plastic strain rate $\dot{p} = (2/3\,\dot{\underset{\sim}{\varepsilon}}^p : \dot{\underset{\sim}{\varepsilon}}^p)^{1/2}$ is identical to $\dot{\lambda}$.

2.2. Kinematic hardening

The back stress is decomposed as a sum of independent variables, in which evolution equation follows the same hardening/dynamic recovery/static recovery format, a generalization of (Armstrong and Frederick, 1966) approach:

$$\underset{\sim}{\mathbf{X}} = \sum_k \underset{\sim}{\mathbf{X}}^{(k)} \qquad \dot{\underset{\sim}{\mathbf{X}}}^{(k)} = \frac{2}{3} C_k \dot{\underset{\sim}{\varepsilon}}^p - D_k \psi_k(\underset{\sim}{\mathbf{X}}^{(k)}) \phi(p) \underset{\sim}{\mathbf{X}}^{(k)} \dot{p} - \left(\frac{J(\underset{\sim}{\mathbf{X}}^{(k)})}{M_k} \right)^{m_k} \frac{\underset{\sim}{\mathbf{X}}^{(k)}}{J(\underset{\sim}{\mathbf{X}}^{(k)})} \tag{5}$$

In its simplest version, function ψ_k contains a threshold effect for the dynamic recovery term:

$$\psi(\underset{\sim}{\mathbf{X}}^{(k)}) = \left\langle J(\underset{\sim}{\mathbf{X}}^{(k)}) - \omega_k \frac{C_k}{D_k} \right\rangle \frac{1}{(1-\omega_k) J(\underset{\sim}{\mathbf{X}}^{(k)})} \tag{6}$$

This threshold is used to improve the modeling capabilities of the classical AF format of the multikinematic hardening model for correctly reproducing ratcheting effects. When this specificity is used, it is necessary to increase the number of back stresses (Chaboche et al., 2012a). Exactly like in the Ohno and Wang (1993) version of this multikinematic hardening model, the post identification with many thresholds is straightforward from the previous knowledge of the classical three back stresses model (without thresholds). However, as ratcheting is not the main fact to be studied in the present paper we limit here the model to the use of only three back stresses without thresholds $\omega_k = 0$; $k = 1, 2, 3$.

2.3. Isotropic hardening

Cyclic hardening or softening can be described through variable R, that can also be decomposed as a sum:

$$R = \sum_k R^{(k)} \qquad \dot{R}^{(k)} = b_k (Q_k - R^{(k)}) \dot{p} \tag{7}$$

where Q_k and b_k are respectively the hardening (softening) saturation state and the rate of convergence to it. In this paper, we do not consider the possibility for a static recovery of isotropic hardening, though it may be necessary for some materials like austenitic stainless steels (Chaboche, 1989; Chaboche and Nouailhas, 1989). In the present model, cyclic hardening or softening may play a role at various places: in the yield stress, using it as a dependent variable $Y(R)$, in the drag stress for the viscoplastic flow, with $K(R)$, in the dynamic recovery term for the back stress evolutions, through $D_k(R)$.

2.4. Strain range memory effect

When necessary, the plastic strain range memory effect (using variable q defined below) is taken into account, playing role on the asymptotic values Q_k of the evolution equations (7). Functions used for $Y(R)$, $K(R)$, $D_k(R)$ and $Q_k(q)$ will be specified in Section 4.

The plastic strain range memory variable q has been introduced by Chaboche et al. (1979), in order to model many of the observed facts for cyclic hardening of 316L Stainless Steels.

Its principle is to progressively store the plastic strain amplitude of a given cyclic plastic strain path. The writing is general, involving a memory surface in the plastic strain space that evolves to follow the current plastic strain in a way that combines isotropic and kinematic evolutions (similar to the hardening rules of rate independent plasticity written in the stress space). The memory surface is expressed as:

$$F = \frac{2}{3} J(\underset{\sim}{\varepsilon}^p - \underset{\sim}{\zeta}) - q \leqslant 0 \tag{8}$$

Scalar q and second rank tensor $\underset{\sim}{\zeta}$ respectively represent the radius and the center of the hypersphere. Their evolution equations are (Chaboche, 1989):

$$\dot{q} = \frac{2}{3} \eta H(F) \langle \underset{\sim}{\mathbf{n}} : \underset{\sim}{\mathbf{n}}^* \rangle \dot{p} \qquad \dot{\underset{\sim}{\zeta}} = \frac{2}{3} (1-\eta) H(F) \langle \underset{\sim}{\mathbf{n}} : \underset{\sim}{\mathbf{n}}^* \rangle \underset{\sim}{\mathbf{n}}^* \dot{p} \tag{9}$$

where the unit normal to the memory surface is given by $\mathbf{n}^* = \frac{3}{2}(\varepsilon^p - \zeta)/J(\varepsilon^p - \zeta)$. So that $\frac{2}{3}\mathbf{n}^* : \mathbf{n}^* = 1$. The Heaviside function is used to have $H(F) = 0$ if $F < 0$ and $H(F) = 1$ if $F = 0$. The McCauley symbol in $\langle \mathbf{n} : \mathbf{n}^* \rangle$ implies that the rates vanish in cases where the current plastic strain rate direction $\mathbf{n}$ is directed inside the memory surface. Consistency condition $F = \dot{F} = 0$ has been used when establishing expressions in (9).

When material parameter η is $1/2$, the scalar variable q immediately attains the maximum plastic strain amplitude experienced. This was the choice made in the first use of this model. The parameter $0 < \eta < 1/2$ was introduced by Ohno (1982) and corresponds to the current use. In this case, memorization of q as the plastic strain amplitude takes a certain number of cycles of the same amplitude, a number that increases for lower values of η. At stabilization, after a few cycles, variable q converges towards the current plastic strain amplitude, denoted $\Delta\varepsilon_p/2$ in uniaxial conditions.

With the formulation (9) the strain amplitude memorization is definitive. For certain applications in which a significant (rapid) cyclic hardening is followed by a (slow) cyclic softening, a memory evanescence term has been added (Nouailhas et al., 1983) in the evolution equation for q:

$$\dot{q} = \frac{2}{3} \eta H(F) \langle \underset{\sim}{\mathbf{n}} : \underset{\sim}{\mathbf{n}}^* \rangle \dot{p} - \xi (1 - H(F)) \langle p - p^* \rangle p^m \dot{p} \tag{10}$$

This evanescence term does not act before a certain amount p^* of accumulated plastic strain has been accumulated. This threshold was not considered in Nouailhas et al. (1983), in which the evanescence was essentially used to model both the 316L stainless steel hardening behavior from its annealed state and its cyclic softening behavior when taken from a heavily wrought bar, without changing any other parameter in the whole model.

2.5. Some previous applications of plastic strain range dependency

The plastic strain range dependency, available through the internal variable q, may be used to describe cyclic hardening of many FCC materials of low stacking fault energy, like OFHC Copper and several Stainless Steels. In these cases the stronger hardening associated with larger strain ranges has been shown to correspond to intragranular dislocation arrangements, including dislocation cells, which size decrease and acuity of walls increases as the strain range is increased or the plastic strain accumulates.

It must be mentioned here that additional effects are observed on these materials, corresponding with the non-proportionality of straining cycles. Cyclic hardening is even more pronounced for out-of-phase loadings than in-phase ones. These facts have been very much studied and documented in the literature since initial works by Lamba and Sidebottom (1978), leading to additional modeling ingredients (Benallal and Marquis, 1987; Tanaka et al., 1987; Krishna et al., 2009).

However such strain range dependencies have also been evidenced for materials that cyclically soften, like Inconel 718 (Chaboche et al., 1991), for which the softening mechanism is related with the shearing of precipitates. More recently the complete constitutive equations described above in Sections 2.1,2.2,2.3,2.4, have been applied to the 9Cr–1Mo ferrito–martensitic steels, in which cyclic softening is very much pronounced and very significantly depending on the applied strain range (Chaboche et al., 2012b). A very important data base and many associated microstructural observations made in Fournier et al. (2006b,a) may give some explanations. The cause of softening seems to be associated with a decrease of subgrain sizes and of dislocation density, but the reason for the strain range dependency is not well elucidated. Recent modeling works based on microstructurally observations, like in Fournier et al. (2011), deliver some additional explanations.

3. Various approaches to model dynamic strain aging effects

Many metallic materials are experiencing DSA effects in some temperature and strain rate domains. First observations of these phenomena have been reported by Portevin and Le Châtelier (1923) in iron and steel between 80 and 250 °C and in aluminum alloys at room temperature, associated with serration observations, which is currently named PLC effect.

Microscopically, these facts result from the dynamic interaction of mobile dislocations and solute atoms. Mobile dislocations move by successive jerks between forest dislocations. Solute atoms then diffuse to dislocations and saturate them while they are temporarily arrested at these obstacles (Van den Beukel, 1975). This mechanism can lead to negative strain rate sensitivity (SRS) in a range of strain rates where dislocations and solute atoms have comparable mobility (Mühlhaus, 1995). If the applied strain rate falls into such an appropriate range and if sufficient interaction between dislocations (via their long-range stress fields) occurs (Zaizer and Hähner, 1997), plastic flow becomes heterogeneous. Plastic strain and plastic strain rate are highly localized in narrow bands in the deformed specimen.

Moreover these inverse SRS effects are often associated with serrations appearing during tensile or compressive tests on uniaxial specimens, corresponding with the propagation along the specimen of discrete bands of localized strain rate.

Introduction of such inverse strain rate effects in macroscopic constitutive models has been proposed in the literature, following various different strategies. We summarize here some of these approaches in the context of cyclic viscoplastic constitutive models. Most of them correspond to the direct introduction of the strain rate at various places in the evolution equations of the different variables.

3.1. MATMOD equations developed by Miller and co-workers

First proposed by Miller (1976), this set of viscoplastic constitutive equations has some differences with the model framework of the present paper. The back stress evolution was only linear in the first version (no dynamic recovery term), but incorporates the static recovery effect with an hyperbolic sine function. There is no yield stress in the model but isotropic hardening is introduced in the drag stress of the viscoplastic flow equation, that uses a combination of an hyperbolic sine and a power function such as:

$$\dot{p} = \theta(T)\left[\sinh\left(\frac{J\left(\underset{\sim}{\sigma}/E - \underset{\sim}{\alpha}\right)}{D}\right)^{\frac{3}{2}}\right]^n \tag{11}$$

where $J(.)$ denotes the von Mises invariant. The back stress $\mathbf{X} = E\,\underset{\sim}{\alpha}$ is normalized by Young's modulus. The main specificity of this model is the drag stress evolution equation, that contains several terms, as in Schmidt and Miller (1981):

$$D = \sqrt{F_{sol,1} + F_{def}\left(1 + F_{sol,2}\right)} \tag{12}$$

where F_{def} is the classical isotropic hardening variable, depending on the accumulated plastic strain. $F_{sol,1}$ and $F_{sol,2}$ are factors depending on the norm of total strain rate (as a parameter), in order to include an explicit representation of solute drag effects and dynamic strain aging, respectively without and with interactions to deformation mechanisms. $\underset{\sim}{\alpha}$ and F_{def} obey a hardening/dynamic recovery/static recovery format in a form similar to (5) but without the threshold. The static recovery terms use also an hyperbolic sine function.

It should be noted that the above quantities are functions of the total strain rate (its norm), which introduces a curious implicit dependency between the viscoplastic strain rate $\dot{p}$ and the viscoplastic strain rate itself, present in $\dot{\varepsilon}$.

Concerning the thermodynamic consistency of this approach, it is sufficient to recall that it obeys the general structure described in Section 2. The fact that isotropic hardening is implemented through the drag stress needs a specific treatment Chaboche (1996), similar to the one indicated in Appendix A. However, the only questionable aspect is the implicit dependency just mentioned above.

3.2. Modification of yield stress and non-linear kinematic hardening

This was proposed in El-Hefnawy et al. (2012) in order to describe some of the DSA effects. It corresponds in fact to the introduction of a function of plastic strain rate in the definition of the yield stress, as well as in the dynamic recovery term of the back stress evolution equation. The yield stress is written as:

$$Y = Y(p) + F_c(\dot{p}) = Y(p) + F_1 \exp(-F_2 |\ln(\dot{p}/\dot{p}_0)|^{F_3}) \tag{13}$$

In this case, we observe the same curious implicit dependency as for Miller's equations. On the other side, the same function $F_c(\dot{p})$ is added to the parameter D of the dynamic recovery.

3.3. The modified VBO theory of Krempl

Viscoplasticity based on Overstress (VBO) was initiated by Yao and Krempl (1985). The main ingredients are slightly different from the ones in the unified viscoplastic constitutive equations developed in the present paper and will be discussed more in detail below. The set of equations presented here are taken from Ho and Krempl (2002) in which is introduced a special term to describe DSA effects.

The VBO theory uses the concept of an equilibrium stress tensor (called $\mathbf{g}$) that corresponds to the material response at an infinitely low rate. It also uses the overstress $\Gamma = J\left(\underset{\sim}{\sigma} - \mathbf{g}\right)$. Compared to our model $\mathbf{g}$ is the sum of the back stress and the yield stress oriented by the current direction of plastic flow $\mathbf{g} = \mathbf{X} + Y\,\mathbf{n}$, and Γ is the viscous part of the stress ($\Gamma = \sigma_v$). We restrict here the theory to the case of a non-volumetric viscoplastic flow, which writes:

$$\underset{\sim}{\dot{\varepsilon}}^p = \frac{\underset{\sim}{\sigma}' - \underset{\sim}{\mathbf{g}}'}{E\,k(\Gamma)} \qquad k(\Gamma) = k_1\left(1 + \frac{\Gamma}{k_2}\right)^{-k_3} \tag{14}$$

where $\underset{\sim}{\sigma}'$ and $\underset{\sim}{\mathbf{g}}'$ are the deviatoric tensors. The evolution equation for the equilibrium stress involves three terms:

$$\underset{\sim}{\dot{\mathbf{g}}} = \psi \frac{\underset{\sim}{\dot{\sigma}}'}{E} + \psi\left(\underset{\sim}{\dot{\varepsilon}}^p - \frac{\underset{\sim}{\mathbf{g}} - \underset{\sim}{\mathbf{f}}}{\lambda A + \beta\Gamma}\dot{p}\right) + \left(1 - \frac{\psi}{E}\right)\underset{\sim}{\dot{\mathbf{f}}} \tag{15}$$

in which $\underset{\sim}{\mathbf{f}}$ is called the kinematic stress and corresponds to the linear kinematic hardening, with:

$$\underset{\sim}{\dot{\mathbf{f}}} = E_t\,\underset{\sim}{\dot{\varepsilon}}^p \tag{16}$$

where the material parameter E_t corresponds to the tangent slope attained asymptotically at significant strains. In (15) ψ is a given function of the overstress Γ, and β a given function of the accumulated plastic strain, for instance

$$\psi = c_1 + (c_2 - c_1)\exp(-c_3\Gamma) \qquad \beta = \beta_1 \exp(-\beta_2 p) + \beta_3 \tag{17}$$

Moreover A is an isotropic hardening variable that may follow exactly the same kind of evolution equation than isotropic hardening variables R in our model:

$$\dot{A} = \omega(A_\infty - A)\dot{p} \tag{18}$$

There are two important differences with our constitutive framework:

- The function ψ of the overstress introduces a rate dependency in the parameters of the kinematic hardening evolution equation. Such a possibility is not considered in the model based on AF rule, which evolution is rate independent, except with the use of the static recovery term.
- The first term, proportional to $\dot{\sigma}$, is a specificity of VBO theory. It allows a very rapid evolution of the equilibrium stress, even in the purely elastic domain. This evolution is driven by the stress, or by the elastic strain. As discussed in Freed and Walker (1990), it introduces some interesting properties for ratcheting prediction capabilities.

The general structure of the VBO theory renders difficult its introduction in a general thermodynamic framework, especially by the direct presence of the first term in Eq. (15) that relates the back stress rate to the elastic strain rate. This point was discussed in detail by Chaboche (1996).

In fact, the VBO model corresponds to the superposition of three back stresses in the context of our model. Such a property may be demonstrated by considering the limiting case of a rate independent version, which can be obtained by taking $k_3 = -1$ and a very small value for k_2 in Eq. (14-b). In that case it corresponds to the decomposition of the equilibrium stress as:

$$\underset{\sim}{\mathbf{g}} = \underset{\sim}{\mathbf{X}} + Y^* \underset{\sim}{\mathbf{n}} = \underset{\sim}{\mathbf{X}}_1 + \underset{\sim}{\mathbf{X}}_2 + \underset{\sim}{\mathbf{X}}_3 + Y^* \underset{\sim}{\mathbf{n}} \tag{19}$$

where Y^* has a constant value and the direction of plastic flow is given by:

$$\underset{\sim}{\mathbf{n}} = \frac{3}{2}\frac{\underset{\sim}{\sigma}' - \underset{\sim}{\mathbf{g}}'}{J(\underset{\sim}{\sigma} - \underset{\sim}{\mathbf{g}})} = \frac{3}{2}\frac{\underset{\sim}{\sigma}' - \underset{\sim}{\mathbf{X}}'}{J(\underset{\sim}{\sigma} - \underset{\sim}{\mathbf{X}})} \tag{20}$$

Replacing (19) into (15), we get, after some easy manipulations:

$$\dot{\underset{\sim}{\mathbf{g}}} = \dot{\underset{\sim}{\mathbf{X}}}_1 + \dot{\underset{\sim}{\mathbf{X}}}_2 + \dot{\underset{\sim}{\mathbf{X}}}_3 \tag{21}$$

where the three back stress rate equations are:

$$\dot{\underset{\sim}{\mathbf{X}}}_1 = \psi\left(\frac{\dot{\underset{\sim}{\sigma}}'}{E} - \frac{\underset{\sim}{\mathbf{X}}_1}{\lambda A + \beta\Gamma}\dot{p}\right) \tag{22}$$

$$\dot{\underset{\sim}{\mathbf{X}}}_2 = \psi\left[\left(1 - \frac{E_t}{E} - \frac{Y^*}{\lambda A + \beta\Gamma}\right)\dot{\underset{\sim}{\varepsilon}}^p - \frac{\underset{\sim}{\mathbf{X}}_2}{\lambda A + \beta\Gamma}\dot{p}\right] \tag{23}$$

$$\dot{\underset{\sim}{\mathbf{X}}}_3 = E_t\dot{\underset{\sim}{\varepsilon}}^p \tag{24}$$

The first variable corresponds to a very special rule, driven by the stress rate in a stress domain that usually corresponds to the elastic domain, but in which the dynamic recovery term is driven by the norm of plastic strain rate. In our model it is replaced by a very rapid Armstrong–Frederick type of back stress evolution, with a great initial slope C_1 but a very rapid saturation (for instance at a plastic strain of about 10^{-4}). The second variable exactly corresponds to a second back stress obeying the AF rule. The third one is a linear kinematic hardening variable.

Function $\psi(\Gamma)$ introduces a significant difference, with a rate dependency of the back stress, that allow additional flexibility in the viscoplastic model capabilities. However, to reproduce DSA and inverse strain rate effects Ho and Krempl (2001) introduced an additional dependency in the dynamic recovery term, with the factor $\lambda A(p) + \beta(p)\Gamma$ at the denominator of the dynamic recovery term.

Considering the asymptotic solution for a constant stress rate (and a constant rate for the equilibrium stress) Ho and Krempl (2001) show the following properties, depending of the value of the β augmentation function:

- $\beta = 0$ corresponds to the standard VBO theory,
- if $\beta = -1$ the model depicts rate insensitivity in the asymptotic state,
- for $\beta > -1$ the model delivers a standard strain rate sensitivity,
- though for $\beta < -1$ it introduces an inverse strain rate sensitivity. However the denominator factor $\lambda A(p) + \beta(p)\Gamma$ must stay positive.

3.4. The model of Yaguchi and Takahashi (2000)

Motivated by the results of an important experimental study on 9Cr–1Mo ferrito–martensitic steel, the initial version of the model is based on the use of two back stresses of the AF format, including static recovery effects. Cyclic softening of the material is described by a reduction of the asymptotic value of the back stress (it corresponds to an evolution of parameters C_k in Eq. (5) instead than playing on the dynamic recovery factor D_k. This cyclic softening modeling also introduces temperature history effects. This part of the model is not developed here, being out of the scope of the present discussion.

In their model Yaguchi and Takahashi (2000) introduce a DSA effect through the development of the yield stress, with:

$$\dot{p} = \left\langle \frac{J(\underset{\sim}{\sigma} - \underset{\sim}{\mathbf{X}}) - R_a}{K} \right\rangle^n \tag{25}$$

R_a is the aging stress, which evolution is given by introducing the plastic strain rate in the asymptotic value R_{as}:

$$\dot{R}_a = b(R_{as}(\dot{p}) - R_a)\dot{p} \tag{26}$$

with:

$$R_{as}(\dot{p}) = A + B\log_{10}(\dot{p}) \tag{27}$$

$$b = \begin{cases} b_r & \text{if } R_a > R_{as} \\ b_h & \text{if } R_a < R_{as} \end{cases} \tag{28}$$

The rate dependency of the aging stress asymptotic value introduces non standard strain rate history effects of two kinds:

- the stress level at the end of a long term (24 h) relaxation test realized after a tensile loading at a strain rate of 10^{-6} s^{-1} is much higher than after a tensile loading at a rate of 10^{-3} s^{-1} (same strain and same duration for the relaxation).
- a two rate tensile test beginning at 10^{-3} s^{-1}, shows in the second part at 10^{-6} s^{-1} a very pronounced stress decrease (similar to a relaxation) followed by a progressive stress increase, before reaching the normal (asymptotic) response of a 10^{-6} s^{-1} test.

Fig. 1, taken from Yaguchi et al. (2002), illustrates the first item and the capability of the model to reproduce it. However, this DSA modeling version has not been used to directly describe inverse strain rate sensitivity in tensile or cyclic tests.

3.5. Physically motivated macroscopic modeling of DSA

The previous models directly introduce the plastic strain rate (or the overstress) in the functions that describe viscoplastic flow and kinematic hardening. Contrarily, the models initiated by McCormick (1988) and Kubin and Estrin (1990) introduce an additional internal state variable t_a, called the effective aging time. The corresponding evolution equations are based on a macroscopic translation of the direct interaction mechanisms between mobile dislocations and the diffusing solute atoms. Explanations given here are taken from Zhang et al. (2001), in which the model principles are clearly summarized.

The non-dimensional solute atoms concentration C_s is assumed to evolve to a saturation value C_m when the effective aging time tends to infinity. However, an important assumption underlying the model (McCormick, 1988) is that the effective aging time is not identical to t_w, the average waiting time a dislocation is arrested at localized obstacles. Following McCormick (1988) the effective aging time t_a is considered to "*relax*" toward t_w with time t, as:

$$\dot{t}_a = 1 - \frac{t_a}{t_w} \tag{29}$$

The waiting time t_w is related to the equivalent plastic strain rate using:

$$t_w = \frac{w(p)}{\dot{p}} \tag{30}$$

where $w(p)$ represents a strain increment produced when all arrested dislocations overcome localized obstacles and move forward to the next pinned configuration (Mühlhaus, 1995). The strain dependence of $w(p)$ may be obtained using a dislocation model.

The relation between the non-dimensional solute concentration C_s and the current effective aging time is most often taken in the form (Ling and McCormick, 1993; Zhang et al., 2001; Bóhlke et al., 2009):

$$C_s = C_s(p, t_a) = C_m[1 - \exp(-P_2 p^{\alpha} t_a^m)] \tag{31}$$

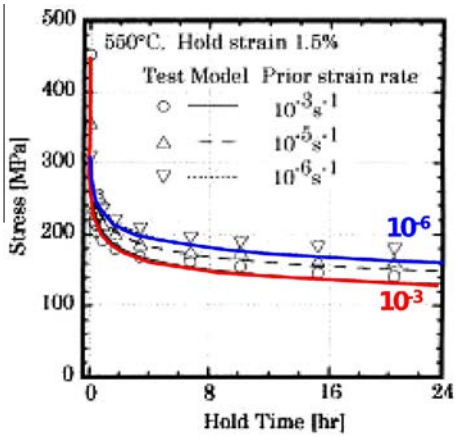

Fig. 1. Inverse relaxation position after different tensile strain rates, for 9Cr–1Mo martensitic steel, and its modeling by Yaguchi et al. (2002).

considering a power dependency on the accumulated plastic strain in the factor that governs rapidity of convergence towards the saturation value C_m. Moreover, the additional resistance to plastic flow is introduced by adding the effect of this current concentration C_s to the current yield stress in the viscoplastic flow equation:

$$Y = \sigma_y + R(p) + R_a(p) = \sigma_y + R(p) + P_1 C_s(p, t_a) \tag{32}$$

where P_1 and P_2 in the two expressions above are usually considered as material constants, though a linear dependency for $C_m(p)$ has been considered by Bóhlke et al. (2009). In the works by Estrin and McCormick (1991) and Mühlhaus (1995) the viscoplastic flow is described by an exponential function of the viscous stress, but the same kind of model may be applied using any other flow equation, like (4).

3.6. Determination of the critical strain before serrations in a tensile test

An interesting development associated with the modeling equations of Section 3.5 is the perturbation analysis that allows to estimate the PLC critical strain, or the strain after which inverse SRS takes place and serrations may appear in a uniaxial tensile test. This can be obtained by analytical manipulations, or in the context of a finite element numerical analysis like in Zhang et al. (2001), Graff et al. (2004), Mazière et al. (2010), Dierke et al. (2007), Benallal et al. (2008), and Belotteau et al. (2009).

Although many similar works have been published with analogous approaches (McCormick, 1988; Kubin and Estrin, 1990; Hähner, 1997), we limit the discussion here to the analytical approach, directly using the set of constitutive equations, following the most recent development by Mazière and Dierke (2012).

Until now such perturbation analyses were made by considering only isotropic hardening, with application to uniaxial loadings on a tensile smooth specimen (with a constant section over the gauge length). In such cases the (uniaxial) stress may be decomposed as:

$$\sigma = \sigma(p, \dot{p}, t_a) = \sigma_y + R(p) + R_v(\dot{p}) + R_a(p, t_a) \tag{33}$$

where $R(p)$ is the isotropic hardening response (it can be obtained by integrating equations like (7)), $R_v(\dot{p})$ is the viscous stress, obtained by inverting viscoplastic flow equations like (4), and $R_a(p, t_a)$ the aging stress in the viscoplastic flow equation. In these works the aging effect is assumed to act only on the yield stress.

There are three levels for the analysis, giving rise to three critical plastic strain estimations. As in Mazière and Dierke (2012) we use the following notations:

$$S = \left.\frac{\partial \sigma}{\partial \ln \dot{p}}\right|_p \quad \text{(steady state SRS)} \tag{34}$$

$$S_i = \left.\frac{\partial \sigma}{\partial \ln \dot{p}}\right|_{p,R_a} = \dot{p}\frac{dR_v}{d\dot{p}} \quad \text{(instantaneous SRS)} \tag{35}$$

$$S_a = \left.\frac{\partial \sigma}{\partial \ln t_a}\right|_p \quad \text{(aging SRS)} \tag{36}$$

$$\Theta = \left.\frac{\partial \sigma}{\partial p}\right|_p = \frac{dR}{dp} + \frac{\partial R_a}{\partial p} \quad \text{(strain hardening modulus)} \tag{37}$$

The *first criterion* (S), is not based on a perturbation analysis and only defines the positiveness of the steady state strain rate sensitivity. This criterion is generally inadequate to detect the occurrence of serrations on the strain–stress curve. Experimental negative strain rate sensitivity has been observed without serrations (McCormick, 1988; Bóhlke et al., 2009).

The *second criterion* (S_{OGC}), is presented in most studies as the relevant one for the occurrence of serrations (Kubin and Estrin, 1990; Hähner, 1997). It is based on a linear perturbation analysis in which a small exponential perturbation is introduced on the set of internal variables, playing role in the constitutive one-dimensional equations. A spectral analysis is performed for the transfer matrix M that links the perturbation of internal variables $(\delta p, \delta t_a)$ with the perturbation of their rates $(\delta \dot{p}, \delta \dot{t}_a)$. Since M is a 2×2 matrix, the spectral analysis can be carried out analytically. The trace of M, its determinant, and its two eigenvalues are computed successively. This second criterion is activated when the real part of the eigenvalues become positive. Indeed it means that the perturbation may follow a growing oscillating evolution (Oscillating Growth Criterion). Detailed calculations are given in Mazière and Dierke (2012). This criterion delivers a larger critical plastic strain than the first criterion.

The *third criterion* (S_{EGC}), called exponential growth criterion, detects when the perturbation may follow a growing but exponential evolution. The eigenvalues previously calculated must be real and positive to ensure such an evolution.

The numerical critical plastic strains extracted from finite element strain/stress curves, and the evolution of the three criteria are plotted in Fig. 2 taken from Mazière and Dierke (2012). In this exercise, the three criteria are tested, using the material model and parameters given in Bóhlke et al. (2009) and finite element simulations of plates in tension. In Fig. 2 the critical plastic strain at the beginning of serrations in a tensile test is reported as a function of the applied strain rate. The FEM results could be considered as numerical experiments, or true serration simulations. The three analytical criteria are applied at the level of equations written at a single material point.

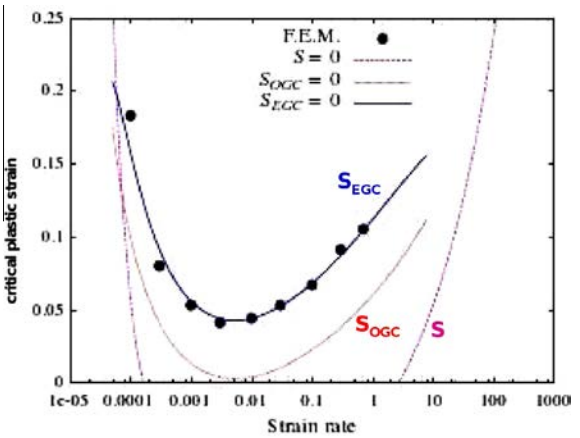

Fig. 2. Critical strain before serrations, as provided by finite element simulations and the three analytical criteria, from Mazière and Dierke (2012).

In this case, the relevant criterion seems to be the exponential one, Ssmall EGC, proposed by Mazière and Dierke (2012), while the generally proposed oscillating one provides predictive but imprecise results.

In the same paper, comparisons are made with experimental results obtained on the AA5775 aluminum alloy, taken from Dierke et al. (2007). They confirm the validity of the third criterion as determining the critical strain at the onset of serrations in tensile experiments at various strain rates (between 10^{-6} and 1 s^{-1}).

4. A set of equations to model Haynes 188 Co base superalloy

4.1. The main experimental observations

As mentioned before, one of the specific observations made for this kind of alloy is the combination, in a large intermediate temperature domain (from 300 to about 800 °C), of a very important cyclic hardening process and of a significant inverse strain rate sensitivity. Literature is already well documented on these two aspects, as shown for instance in Fig. 3 realized from the results of Rao et al. (1995) and Rao et al. (1997). The main observation is that the increase of the maximum stress at each cycle is approximately linear with the logarithm of the number of cycles (at a given temperature, with a total strain range of 0.8% and at a given strain rate of 10^{-3} s^{-1}). When plotted as a function of the accumulated plastic strain, the same results show a power like evolution, which is somewhat non usual, with no tendency to really stabilize, except just before failure (due to damaging effects and crack growth).

The other fact, from the same publications is the inverse strain rate dependency, by comparing the previous results with similar tests realized at 10^{-4} s^{-1}. In the temperature domain from 300 to 700 °C the maximum stress evolution with the applied number of cycles is similar, but with significantly higher stress levels. Other tests with rate changes at some intermediate cycles do confirm this inverse rate sensitivity. Similar observations have been made on several other superalloys used in combustion chambers (not necessarily Co based).

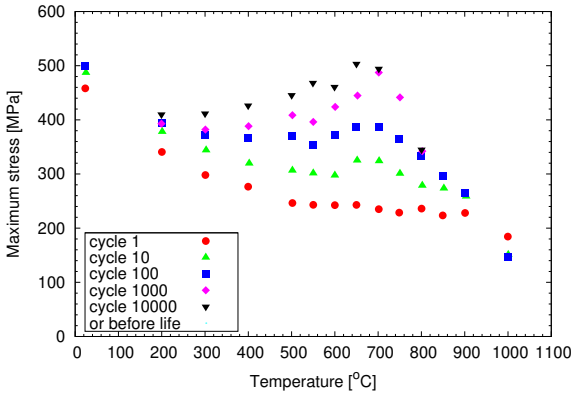

Fig. 3. Cyclic maximum stress responses as a function of temperature for Haynes 188 superalloy, strain amplitude 0.4%, strain rate 10^{-3} s^{-1}, reproduced from Rao et al. (1997).

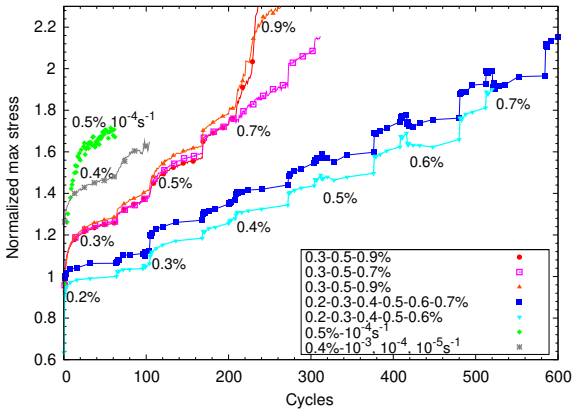

Fig. 4. Multilevel cyclic tests on Haynes 188 at 600 °C (maximum stress normalized by the 0.2% yield stress).

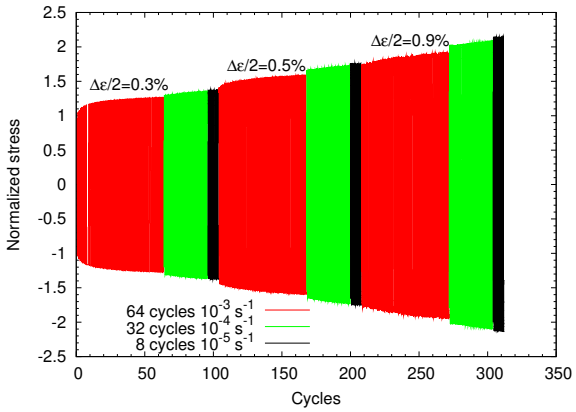

Fig. 5. Example of stress response in a test with three levels at three successive strain rates at 600 °C.

More recently, a significant series of multilevel experiments has been realized at Snecma on Haynes 188, in the whole temperature domain, which only few results are shown here. As unpublished results they are plotted only in a normalized form in Fig. 4. Tests are conducted in tension–compression under strain control. At each strain amplitude are successively applied 64 cycles at 10^{-3} s^{-1}, followed by 32 cycles at 10^{-4} s^{-1}, then by 8 cycles at 10^{-5} s^{-1}. Successive strain amplitudes are 0.3%, 0.5%, 0.7% in one of the typical tests, and levels 0.2%, 0.3%, 0.4%, 0.5%, 0.6% and 0.7% in another series (not shown on the figure). Fig. 5 illustrates the complete response for one of these tests (normalized stress response as a function of cycles.

Typically, at 600 °C three observations can be made from the shown tests (well reproduced in three different identical tests):

- at each level we have a cyclic hardening, with a progressive increase of the maximum stress,
- at a fixed level of strain amplitude (0.3% then 0.5%) we clearly observe the increase in the maximum stress, both at the transition from 10^{-3} to 10^{-4} s^{-1} and then, more pronounced, from 10^{-4} to 10^{-5} s^{-1}, showing a significant inverse SRS,
- when changing the strain amplitude level (from 0.3% to 0.5% and from 0.5% to 0.7%) we clearly observe a progressive increase of the maximum stress, though it was much less rapidly increasing at the previous level. This is a manifestation of a dependency of the cyclic hardening rate to the current plastic strain range.

For comparison, this test at 600 °C is reproduced in Fig. 6 together with similar tests at 20, 700, 800, 900 °C. The figure shows classical rate dependency at 20 and 900 °C, the inverse strain rate dependency at 700 °C (compared to 600 °C the maximum stress increase is less pronounced at the transition from 10^{-3} to 10^{-4} s^{-1} but more pronounced from 10^{-4} to 10^{-5} s^{-1}). At 800 °C we have a mixed behavior: no rate dependency from 10^{-3} to 10^{-4} s^{-1} (at the first level) and a standard decrease of the maximum stress from 10^{-4} to 10^{-5} s^{-1}. At all temperatures except 900 °C we observe the dependency of the cyclic hardening rate to the applied strain range.

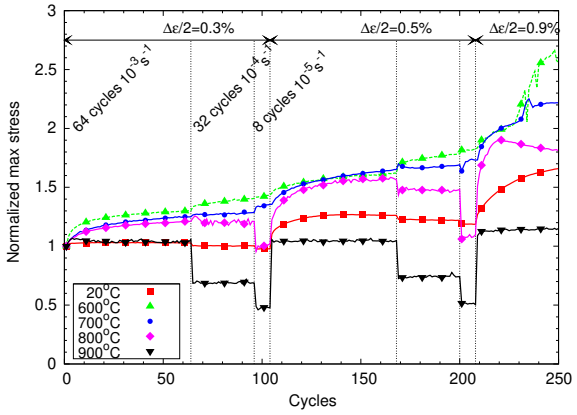

Fig. 6. Multilevel cyclic tests at different temperatures (normalized by the maximum stress at the first cycle).

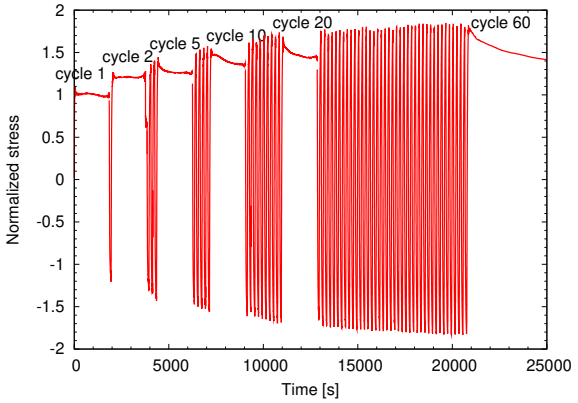

Fig. 7. Cyclic test at 600 °C involving hold periods at cycles 1, 2, 5, 10, 20 and 60. Strain amplitude: 0.5%, strain rate: 10^{-4} s^{-1}.

Another kind of test is shown in Fig. 7, that reports the stress-time response in a 600 °C test made at a 10^{-4} s^{-1} strain rate and a 0.5% strain amplitude, in which 30 min. hold periods are applied at the maximum tensile strain for cycles 1, 2, 5, 10, 20 and 60 (the relaxation at cycle 60 is over 15 h). From this test it is clearly observed that cyclic hardening influences much more the viscous part of the stress (or overstress) than the yield stress. The relaxation is practically negligible at the two first cycles but the amount of stress to be relaxed increases progressively, in parallel with the increase in the maximum stress.

4.2. The main ingredients of the constitutive model

The model obeys the general structure defined in Section 2. It is still presented in its isothermal form. Its generalization for non-isothermal situations is classical and straightforward (Chaboche, 2008). In the present application we use the following specificities:

- the hyperbolic sine function (4) for the viscoplastic flow,
- three back stresses for the kinematic hardening, without thresholds ($\omega_1 = \omega_2 = \omega_3 = 0$), but including static recovery as in (5),
- the plastic strain rage memory variable q, with the following dependencies for the asymptotic values of the isotropic hardening variables:

$$Q(q) = Q_0 + (Q_M - Q_0)\exp(-2\mu q) \tag{38}$$

- the classical isotropic hardening, with three scalar R_i variables, for which the asymptotic values are proportional to $Q(q)$ (the ζ_i are the proportionality factors):

$$R = \sum_i R^{(i)} \qquad \dot{R}^{(i)} = b_i(\zeta_i Q(q) - R^{(i)})\dot{p} \tag{39}$$

- the non classical dynamic strain aging processes are described through the McCormick type of approach presented in Section 3.5, using the effective aging time t_a, which evolution equation is:

$$\dot{t}_a = 1 - \frac{t_a}{w(p)}\dot{p} \tag{40}$$

where function $w(p)$ is assumed to be linear in the accumulated plastic strain: $w(p) = w_1 + w_2 p$
- the corresponding aging stress is defined using an approach similar to the one used by Yaguchi and Takahashi (2000), with its asymptotic value defined as:

$$R_{as}(R, t_a) = P_1(C_1 + C_2 R)(1 - \exp(-P_2 t_a^m)) \tag{41}$$

and the evolution equation like:

$$\dot{R}_a = b_a(R_{as}(R, t_a) - R_a)\dot{p} \tag{42}$$

We may select two different values for the rapidity of evolutions: $b_a = b_h$ if $R_a < R_{as}$ and $b_a = b_r$ if $R_a > R_{as}$. In (41) we did not consider the power dependency in p like in (31), but prefer to introduce a dependency in the current cyclic hardening state through the variable R. This is really necessary when modeling cyclic tests, as p accumulates and may attain very high values. Figures of next section clearly show that increasing the factor before the t_a^m in (41) completely changes the rate domain where inverse SRS takes place.
- the classical isotropic hardening and the aging stress may influence several factors in the constitutive model, using:

$$\begin{aligned} Y &= k + (1 - \xi)(R + R_a) \\ K &= K_0 + \xi(R + R_a) \\ D_k &= \frac{D_{k0}}{1 + \beta R} \end{aligned} \tag{43}$$

where k, K_0 and D_{k0} are the initial values of Y, K, D_k respectively. In the present version of the model, we do not consider necessary to take into account the DSA effect on the evolution equation of the back stresses. It is clear that such a choice could be difficult to justify from a physical point of view, as the back stress are related, at least partly, with dislocation movements and can be influenced by solute atoms. However, as no experimental data was showing evidence of such a coupling effect, we have considered this simplifying assumption. Introducing the coupling of the back-stress with the aging stress could be the subject of a future development in order to improve the capabilities of the model.

With these various ingredients, under uniaxial loading conditions, the current stress may be decomposed as follows:

$$\sigma = \sum_k X^{(k)} + \left[(1 - \xi)(R + R_a) + (K_0 + \xi(R + R_a))\left(\mathrm{Asinh}\left(\frac{\dot{p}}{\dot{\varepsilon}_0}\right)\right)^{1/n}\right] \tag{44}$$

in which the sign before the bracket indicates tensile $(+1)$ or compressive (-1) plastic flow.

Considering the thermodynamic aspects, the fact that isotropic hardening variables (R and R_a) appear in the yield stress and in the drag stress (at the denominator of the viscoplastic flow equation (4) needs some specific treatment, as detailed in Appendix A.

The model has been implemented within the Finite Element software Z-SET Zebulon (2011). An explicit second order Runge Kutta time integration scheme with automatic time stepping is used to solve evolution equations. Work is underway to implement a more robust time integration method. The chosen MacCormick approach to model DSA allows the simulation of serrations and associated localization bands in complete FE structure calculations as it has been emphasized in Section 3.6. This point will not be addressed in the present contribution.

4.3. Model identification method

The procedure is discussed for the more complicated case, at 600 °C, where the various physical processes are interacting all together. As usual in the identification steps of the parameters of unified viscoplastic constitutive models (Chaboche, 2008), we may separate them into three successive phases:

The rate independent version, in order to obtain a first evaluation of kinematic and isotropic hardening effects, using data with approximately the same strain rate, for instance $\dot{\varepsilon} = 10^{-3}\ \mathrm{s}^{-1}$:

- Step 1: adjustment of kinematic hardening parameters on more or less stabilized conditions. Even if a true stabilization does not occur, a pseudo-stabilized cyclic curve can be defined from data after a sufficiently large number of cycles, and the shape of stress–strain loops is also available.
- Step 2: from the maximum stress evolutions under reversed strain controlled cyclic tests (constant or multiple level tests), we obtain an evaluation of the asymptotic values $Q(q)$ corresponding to different plastic strain amplitudes $q = \Delta\varepsilon_p/2$. The dependency is quantified from the different rates observed from the plot of σ_{Max} as a function of the accumulated plastic strain (in a semi-logarithmic scale).

Let us remark here that, with a material behavior like for Haynes 188 at 600 °C, the plastic strain amplitude is significantly decreasing due to the continuous cyclic hardening. The measurement of the accumulated plastic strain is then defined from the obvious uniaxial expression of amplitudes under a total strain control:

$$\frac{\Delta\sigma}{2} = E\left(\frac{\Delta\varepsilon}{2} - \frac{\Delta\varepsilon_p}{2}\right) \tag{45}$$

where $\Delta\varepsilon$ is the imposed quantity, $\Delta\sigma$ the measured one, and $\Delta\varepsilon_p$ is determined if we consider Young's modulus as a known quantity. From a fitting of the experimental response $\Delta\sigma(n)$ at cycle n it is easy to obtain $\Delta\varepsilon_p(n)$, then to approximate the accumulated plastic strain by:

$$p(N) = 4\sum_{n=1}^{N}\frac{\Delta\varepsilon_p(n)}{2} \tag{46}$$

- *Step 3*: the parameters b_i for the three isotropic hardening variables are also determined from the measured stress amplitudes (or maximum stress) as a function of the accumulated plastic strain. Let us remark that three such variables are needed as we continue to use an exponential rule like obtained from (7), though cyclic hardening extents on a very large number of cycles. As for kinematic hardening, the use of three variables may be considered as a development of a power law kind of dependency (power relationship between the stress in excess of the back stress and the accumulated plastic strain).
- *Step 4*: the classical isotropic hardening variable R may be applied at three positions in the model, following (43). Separating between Y and K is not possible at present (because only a fixed strain rate is considered). However we may determine the parameter β in the back stress evolution equation (assumed to be the same for the three back stresses). It comes from the comparison of the measured stress–strain loops between the first cycle and the pseudo stabilized one, in the same tests as previously. From them, it clearly appears that cyclic hardening has a significant influence on the instantaneous slope, that is on the kinematic hardening;
- *Step 5*: All the parameters of the rate independent model are now determined. However a first re-adjustment step must be performed (eventually using a systematic optimization procedure), as the parameters determined in steps 1 to 4 are not really independent. At each step we determine a first rough approximation of the corresponding parameters, but we need to iterate in order to refine the evaluation.

The rate dependency of the model can be determined now (without static recovery), using the tests with various strain rates (10^{-3}, 10^{-4}, 10^{-5} s^{-1}) and the relaxation tests. In this step the long term relaxation, with plastic strain rates below 10^{-8} s^{-1}, is not considered. As the rate effects have two different origins, the classical power dependency and the DSA effect, it is the really difficult step.

Let us first examine the role of the main parameters in the DSA part of the model. This is done by means of the asymptotic model response corresponding to test conditions involving a fixed plastic strain rate $\dot{p}$, and for a given value of the accumulated plastic strain p. In this case, we easily get the analytical solution (under the approximation of a constant value for $w(p)$):

$$t_a = \frac{w(p)}{\dot{p}}\left[1 - \exp\left(-\frac{p}{w(p)}\right)\right] \tag{47}$$

Then, as a first approximation, when w is small enough, w and P_2 play the same role in equation (41) but less rapidly for w (which acts through t_a^m). They both translate the R_a curve in the plastic strain rate, as shown in Fig. 8. On the other side,

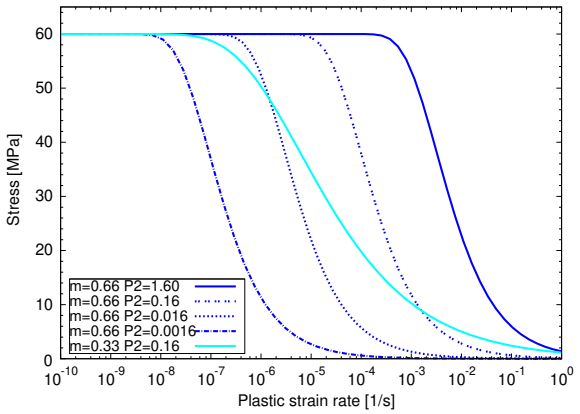

Fig. 8. Evolutions of the aging stress with the plastic strain rate for $m = 0.66$ and $m = 0.33$ and various values of parameter P_2.

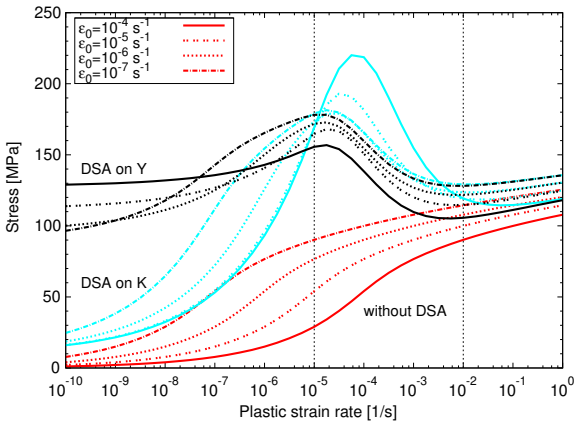

Fig. 9. Evolutions with plastic strain rate of the normal viscous stress as well as the total stress for the additive or multiplicative solutions for introducing the aging effect.

exponent m defines the size of the rate domain in which the negative rate sentitivity takes place. Comparing the two values proposed in the literature (Mesarovic, 1995), $m = 0.66$ and $m = 0.33$, we observe in Fig. 8 that $m = 0.33$ induces a much larger domain for negative SRS, much too large compared to available experiments on Haynes 188. Therefore, in order to fix the inverse SRS domain between 10^{-5} and 10^{-2} s^{-1}, we select values $m = 0.66$, $w = 0.0004$ and $P_2 = 0.40$.

Let us note that other combinations of w and P_2 would deliver similar results, but w describes a delay to aging effect, then it is a sensitive parameter for the critical strain before serrations, an application not considered in the present paper.

Now, we have to superimpose the DSA effect to the normal viscosity effect. In Fig. 9 we compare the two extreme cases for the stress decomposition, by means of simple analytical solutions, by using (47) in (41), considering the immediate saturation of (42) (using large values for b_a), and reporting the result into (43). The accumulated plastic strain is assumed constant and the classical hardening variable R is considered as zero valued. Moreover the back stress takes a very small value of 20 MPa and the initial drag stress is $K_0 = 50$ MPa. The figure shows why it is better to use the hyperbolic sine function (4) with a low valued $\dot{\varepsilon}_0$ parameter ($\dot{\varepsilon}_0 = 10^{-6}$ or 10^{-7} s^{-1}), in order to limit the normal rate dependency in the rate domain where the inverse SRS takes place (10^{-5} to 10^{-2} s^{-1} in our case). More or less arbitrarily the power law exponent is fixed at $n = 3.5$. It could be adjusted later for very low rates when also using the static recovery.

The exercise is made with four values of the parameter $\dot{\varepsilon}_0$ (10^{-4}, 10^{-5}, 10^{-6}, 10^{-7} s^{-1}), and the aging stress is automatically adjusted (by parameter P_1) in order to impose a given stress difference between the two strain rates 10^{-5} and 10^{-2} s^{-1}. This difference is taken as 50 MPa, a good average of several experimental data.

The lower curves correspond to the viscous stress, described by the hyperbolic sine term in (45) for the case with $R_a = 0$. The two other sets of curves are the limit cases where the DSA does affect the yield stress ($\xi = 0$) and the one were it does affect the drag stress ($\xi = 1$). Two observations can be made:

- introducing DSA effect in the yield stress (additive choice) allows to well represent the negative SRS regime, but for lower strain rates the stress relaxation possibilities are totally limited by the aging stress;
- contrarily, introducing DSA effect on the viscous stress (multiplicative choice) allows a much better relaxation at small strain rates but, to respect the inverse SRS effect (that we imposed) the parameter $\dot{\varepsilon}_0$ must be chosen very low, in order to benefit of the saturation regime of the hyperbolic sine function (above 10^{-5}). For larger $\dot{\varepsilon}_0$, to respect the constraint (the stress difference between 10^{-5} and 10^{-2} s^{-1}) the aging stress must be greatly increased, leading to an exaggerated peak between 10^{-5} and 10^{-4} s^{-1}.

Having fixed the standard viscosity ($n = 3.5$, $\dot{\varepsilon}_0 = 10^{-7}$ s^{-1}, $K_0 = 50$ MPa), the parameters $\xi = 1$, $C_1 = 8$, $C_2 = 0.7$ are then adjusted to recover both an inverse strain rate dependency in the cyclic tests at 10^{-3}, 10^{-4}, 10^{-5} s^{-1} and a correct beginning of the relaxation realized at cycle 60 of the test at 0.5% strain amplitude and 10^{-4} s^{-1}, which experimental points are indicated in Fig. 10. Below 10^{-7} s^{-1} a correct adjustment is not searched in the relaxation test, as static recovery of the back stress is still necessary to describe long term relaxation. At this stage it is observed that $\xi = 1$ is really a sufficient assumption, with cyclic hardening and DSA playing role only on the viscous part of the stress.

Static recovery. The last step in the identification is to determine the parameters for static recovery of the back stresses. This is done from the long relaxation tests available, in particular the one after 60 cycles in the test at 0.5% strain amplitude and 10^{-4} s^{-1}. A last check may be performed by the estimation of some available tensile creep tests. Figures in the next section will illustrate the corresponding capabilities.

The practical identification process of such a complicated model is a complex procedure. It cannot be argued that we have uniqueness of the set of obtained parameters, nor that we obtain "the best set". Some of the parameters are fixed more or

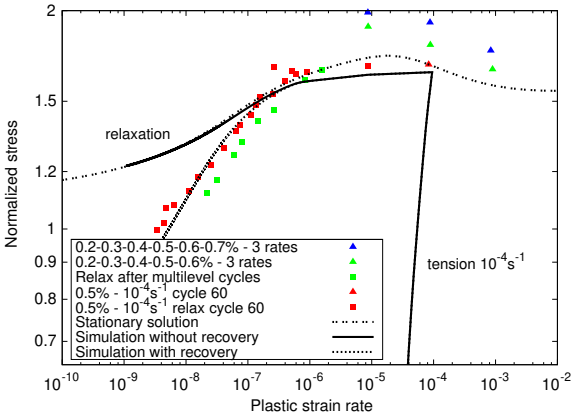

Fig. 10. Experimental results and calculated ones for the stress as a function of plastic strain rate. The red curve corresponds to the analytical asymptotic solution, the black one to the numerical simulation of the test with tensile strain rate of 10^{-4} s^{-1}, without static recovery. (For interpretation of the references to color in this figure legend, the reader is referred to the web version of this article.)

less arbitrarily, as described above in the successive steps. After these arbitrary choices, the other parameters are identified by automatic error minimization techniques. In this work we used the very friendly software Z-SimOpt (graphical simulation and optimization system), available in our Z-SET platform Zebulon (2011). At this step, uniqueness can be controlled, but it is submitted to the choice made of the test data that enter into this minimization process (and their corresponding weights). This kind of difficulty is common to any such complex constitutive model.

5. Assessment of the constitutive model capabilities at 600 °C

As indicated in Section 4.3 the model exploitation has been done with the following particularized version:

- without the delay effect on the aging stress R_a introduced by Eqs. (41) and (42) from Yaguchi et al. (2002), i.e. using a very large value for b_a, so that $R_a = R_{as}(R, t_a)$;
- without the influence of aging stress on the back stress evolution equations, but taking into account the classical cyclic hardening by variable R, as indicated in (43-c);
- without any evolution of the yield stress, with $\xi = 1$ in (43-a),
- the effect of R_a is only introduced in the viscous part, using the drag stress $K = K_0 + R + R_a$.

It means that, except the classical parameters for the constitutive equations (describing kinematic hardening and isotropic hardening with plastic strain range memorization) we only have the following additional parameters in the present version:

- β, to describe the influence of isotropic hardening on the back stresses,
- P_1C_1 and P_1C_2 to introduce the DSA effect on the viscous stress,
- P_2 and m to define the aging stress,
- w_1 and w_2 in the waiting time definition by function $w(p)$ in (40) but, in the exploitation, we used $w_2 = 0$.

Fig. 11 shows the obtained results for the simulation of the test at 10^{-4} s^{-1} that incorporates hold periods of 1/2 h at maximum strain ($\varepsilon_{max} = \varepsilon_{min} = 0.5\%$). It shows the comparisons on the stress relaxation during each hold period at cycles 1, 2, 5, 10, 20, 60. In Fig. 12 is also presented the complete simulation for the 15 h relaxation at cycle 60. It is quite well reproduced as taking into account the static recovery of the kinematic hardening variables. Let us note that this test has been used to fit the parameters of the static recovery.

Fig. 13 reports a number of multilevel cyclic tests that allow to check both the cyclic hardening description and the capability to correctly reproduce the inverse strain rate effects and their evolution with cyclic hardening. The longer tests are with six successive strain amplitude levels, from 0.2% to 0.7%, with three successive strain rates at each level, as explained in Section 4.1. The two quasi identical tests are quite well reproduced for the maximum stress increase when increasing the strain amplitude from 0.2% to 0.3% and 0.4%, due to the increase of the back stress and of the isotropic hardening (thanks to the plastic strain range memory effect). The increases when changing the rate from 10^{-3} to 10^{-4} s^{-1} or from 10^{-4} to 10^{-5} s^{-1} are also well reproduced both at the beginning but also after significant cyclic hardening. A much important fact is also observed and well described for the three largest strain amplitudes; when changing the amplitude from 0.5% to 0.6%, then 0.6% to 0.7%, there is a sudden decrease in the maximum stress (instead of an increase). This is typically due to the negative SRS

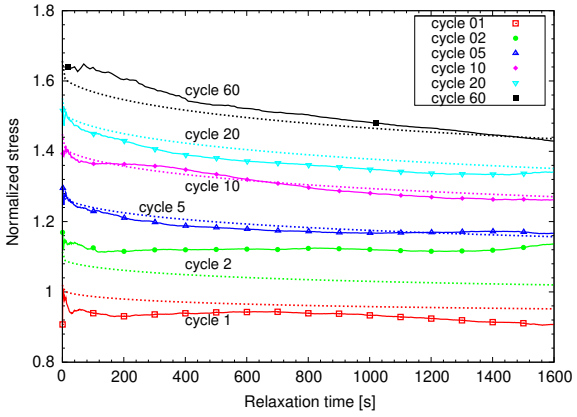

Fig. 11. Simulation of stress relaxation curves during 1/2 h hold times in the test at 0.5% and 10^{-4} s^{-1}.

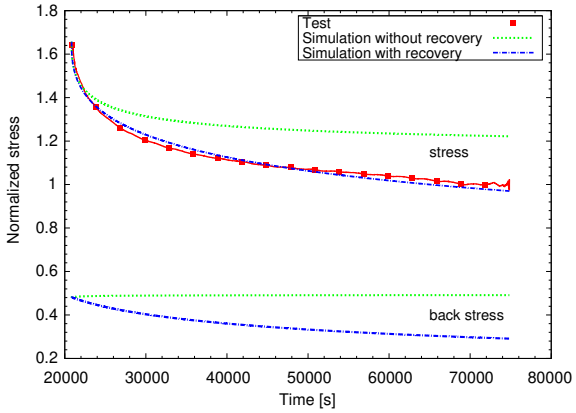

Fig. 12. Simulation of 15 h relaxation at cycle 60, with and without static recovery.

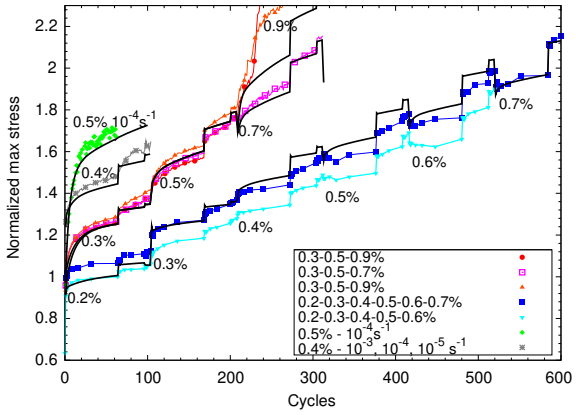

Fig. 13. Simulations of multilevel cyclic tests, with three successive strain rates at each level. Dotted lines: without taking the initial hardening into account (the simulations are with the continuous black lines).

(changing the rate from 10^{-5} to 10^{-3} s^{-1}). At the lower strain amplitudes (0.2–0.4%), increasing the strain amplitude of 0.1% increases quite a lot the maximum back stress. For larger strain ranges, due to the non-linearity of kinematic hardening, the increase of 0.1% produces a much lower increase of the maximum back stress but at the same time the aging stress is much larger due to cyclic hardening, giving rise to an increasing negative jump of the maximum stress when changing the rate from 10^{-5} to 10^{-3} s^{-1}. These trends are clearly observed in the test results.

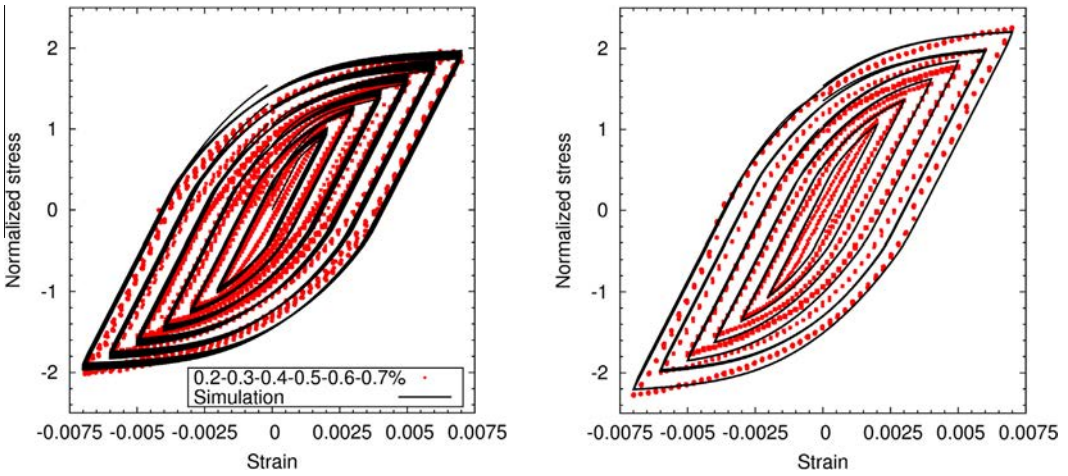

Fig. 14. Simulation of stress strain loops multilevel test 0.2–0.3–0.4–0.5–0.6–0.7% at 10^{-3} s^{-1} (left) and 10^{-5} s^{-1} (right).

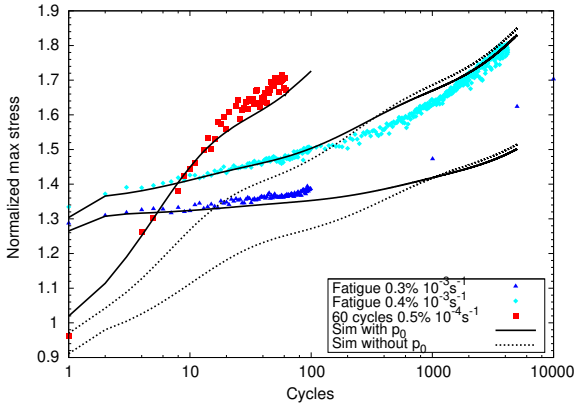

Fig. 15. Simulation of the fatigue tests over a large number of cycles, with (solid lines) or without (dotted lines) taking into account the initial hardening.

The three tests just above, with three successive levels (0.3%, 0.5%, 0.7%) are also well described, showing the same trends than for the previously described ones. Let us note that, contrary to the previous ones, these quasi identical tests were used to determine the parameters of the constitutive model. Another test at 0.4% strain amplitude is still well predicted, for the three rates (still showing the negative SRS). The upper curve corresponds to the test at 0.5% amplitude and 10^{-5} s^{-1} strain rate (with some hold times) and is well reproduced for the maximum stress evolution.

In Fig. 14 are compared the stress–strain loops of one of the tests with six strain levels. On the left we have the part of the test (and simulation) corresponding to the rate 10^{-3} s^{-1}, on the right the one corresponding to 10^{-5} s^{-1}.

In Fig. 15 are reported the comparisons over much larger number of cycles (on a logarithmic scale), where two fatigue tests under 10^{-3} s^{-1} (amplitudes of 0.3% and 0.4%) are well reproduced until about 3000 cycles (the test at 0.4% failed at about 5400 cycles). The test shown previously at 0.5% amplitude and 10^{-5} s^{-1} is reported for comparison, showing a much more rapid cyclic hardening, partly due to the lower rate, but also due to a problem related with the initial hardening of the other tests, that we discuss now.

The two fatigue tests shown in Fig. 15 are well described with the same material parameters because it was introduced an initial hardening for each test. Specimens came from different origins, with different processing routes and, though submitted to the same heat treatments, they show significantly different initial strengths, measured by the 0.2% monotonic yield stress. In the present modeling work we decided to incorporate these test in the study by only modifying the initial value of the accumulated plastic strain, $p_0 = p(0)$, which changes consistently the initial value of the isotropic hardening variables $R^{(k)}$, using:

$$R_0^{(k)} = \zeta_k Q_0 (1 - \exp(-b_k p_0)) \tag{48}$$

The test simulations are done with the same model, using $R^{(k)}(0) = R_0^{(k)}$ in Eqs. (39) instead of $R^{(k)}(0) = 0$. The simulations made in Fig. 15 (with solid lines) were done for the two fatigue tests by using $p_0 = 2.0$. The dotted lines indicate the simulations when $p_0 = 0$, showing significant differences before 200–800 cycles.

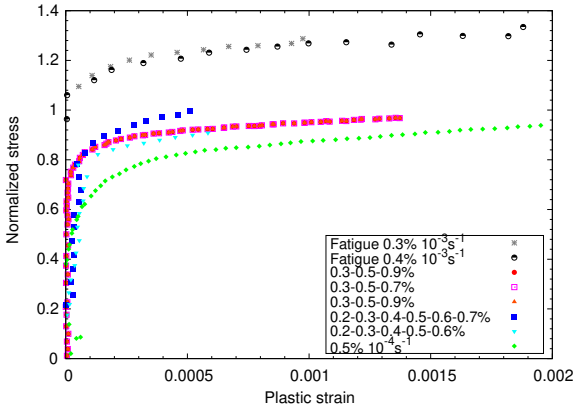

Fig. 16. First monotonic response of the various cyclic tests at 600 °C, showing the need to take into account different initial hardening states.

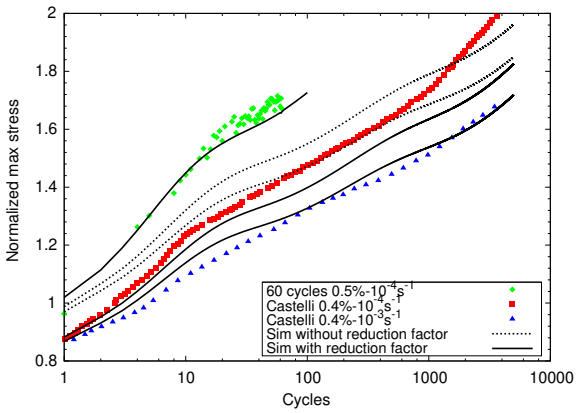

Fig. 17. Simulation of two tests from the literature. Dotted lines: with the same parameters and solid lines: with a reduction factor of 0.89.

On the multilevel tests of Fig. 13 the chosen initial values were $p_0 = 0.08$ for the 6 level tests, $p_0 = 0.04$ for the three levels tests and $p_0 = 0.22$ for the test with three rates at 0.4% strain amplitude. p_0 was taken zero in the test at 0.5% and 10^{-4} s^{-1}.

As shown in Fig. 16, where are reported the experimental first monotonic curves of these tests, the differences in the initial resistance obtained by (48) and the respective values chosen for p_0 are well in accordance with the differences in the measured monotonic 0.1% proof stress.

Taken from the literature (Rao et al., 1995; Rao et al., 1997), two additional fatigue tests are simulated, which results are shown in Fig. 17. They are strain controlled tests under a 0.4% strain amplitude, at two strain rates, 10^{-3} s^{-1} (the lower maximum stresses) and 10^{-4} s^{-1} (the larger stresses). For comparison the tests with 0.5% strain amplitude at 10^{-4} s^{-1} is also reproduced. Using the same parameters as before delivers slightly higher predictions (the dotted lines), indicating that the different origin and production process of this old batch of material was giving a little less resistant material. However, by simply applying a multiplicative factor of 0.89 to all the stress parameters in the model (K_0, k, Q_0, Q_{sat}, C_k, P_1C_1) we may obtain a much better response for the two rates. Such a result looks quite satisfactory and promising for the extensibility of the model to other batches or other similar materials.

Thanks to the use of a DSA modeling framework based on the McCormick aging time variable, the present model has the capability to simulate the serrations in uniaxial tests, under monotonic and cyclic conditions, as well as their evolution with cyclic hardening. This may be done either by predicting the critical strain before serrations through an analytical approach like the one indicated in Section 3.6, or by performing complete FE simulations able to reproduce strain rate localization PLC bands as in the works by Zhang et al. (2001), Dierke et al. (2007), Benallal et al. (2008), and Belotteau et al. (2009). Such developments will be considered in future works.

6. Concluding remarks

This paper is concerned by the constitutive modeling of materials that exhibit simultaneously a very pronounced (and slow) cyclic hardening and a significant dynamic strain aging that promote a negative strain rate sensitivity. This is often

the case of materials used in combustion chambers of jet engines, especially in the intermediate temperature domain, from 300 to 800 °C.

The existing tension–compression experiments published in the literature for a material like Haynes 188 superalloy have been completed by special multilevel cyclic tests that offer many additional informations.

Modifications are proposed for an existing viscoplastic constitutive modeling framework, that have the potential to well describe the combination of these cyclic hardening and dynamic strain aging effects. Compared to other older modeling efforts, in the context of unified viscoplastic models, the proposed approach differs in using an additional state variable, the effective aging time, physically motivated by following arguments in McCormick approach.

Let us mention that previous works in the literature using such an effective aging time and the corresponding evolution equation were limited to monotonic plastic (or viscoplastic) flow, with low hardening effects. In the present case the constitutive model is able to reproduce quite well the extremely pronounced cyclic hardening of the material, including its dependency to the applied strain amplitude as well as to the strain rate.

One of the particular choices made in this work was to incorporate the aging effect in the viscous part of the stress, instead of using an additive aging stress. This allows to correctly reproduce the limited stress relaxation before cyclic hardening and the increase of the stress relaxation (for identical hold periods) when the cyclic hardening evolves. Moreover the long term relaxation tests are well described, thanks to the use of a very low yield stress and of the static recovery of the back stresses, a classical ingredient of the previously existing framework.

Several aspects should be addressed in the near future concerning the validation and exploitation of the proposed modified framework:

- to confirm its capabilities for other temperature levels, in order to get a completely exploitable set of material parameters,
- to introduce additional couplings, such as the possible role of the aging stress in the back stress evolution equation, associated with some special tests involving indirect measurements of the back stress,
- to compare estimations made under cyclically varying temperature conditions, under stress or mechanical strain control, with some available uniaxial test results,
- to use the obtained constitutive equations for the cyclic inelastic analysis of some structural components, showing the impact of the new formulation against the results obtained with the classically used models, that neglect cyclic hardening and dynamic strain aging,
- to exploit the analytical and numerical methods for the determination of the critical strain before serrations (in tension–compression tests), taking into account both kinematic hardening, cyclic hardening and inverse strain rate sensitivity.

Acknowledgements

Cooperation with Snecma, Turboméca and Centre d'Etudes Aéronautiques de Toulouse (CEAT) during the Program "PRC Structures Chaudes" is gratefully acknowledged, especially for the availability of the experimental data bases on the Haynes 188. Financial support by the French Ministry of Transportation (Direction des Programmes de l'Aviation Civile) and of the French Ministry of Defence (Délégation Générale à l'Armement) is also gratefully acknowledged. A special mention should be made concerning the fruitful discussions and suggestions by S. Forest from the Centre des Matériaux of Mines-ParisTech.

Appendix A. On the thermodynamic consistency of the constitutive model

We briefly describe here the way by which the constitutive model developed in the present paper may be written in order to meet the thermodynamic requirements, in particular the Second Principle. The general framework is standard, introducing a thermodynamic state potential, that depends of independent state variables, and an associated set of thermodynamic forces that derive from this potential. The interested reader is invited to refer to Lemaître et al. (2009) and Chaboche (1996, 1997). In what follows we introduce only the main ingredients that are needed to check the positiveness of the dissipation (Second Principle), without considering the terms associated with thermal dissipation. In order to simplify the present discussion, we consider only one back stress in the model and one isotropic hardening variable (that obeys equation like (39)). Moreover, we consider the plastic strain range memory variable q as playing role of a parameter, so that in what follows Q is taken like a constant. As the current aging stress obeys a similar evolution equation (42), the following proof will apply similarly. In the present case the state variables are the strain (elastic one), the backs strains α, the scalar variables r and δ for isotropic hardening. The role of these two variables will be understood later. The thermodynamic state potential is the free energy

$$\psi = \psi_e(\underset{\sim}{\varepsilon}^e) + \psi_p(\underset{\sim}{\alpha}, r, \delta) \tag{A.1}$$

The first term is the elastic energy and gives rise to Hooke's Law. The second one is the energy stored by kinematic and isotropic hardening. The thermodynamic forces are defined by:

$$\underset{\sim}{\mathbf{X}} = \frac{\partial \psi}{\partial \underset{\sim}{\alpha}} \qquad \overline{R} = \frac{\partial \psi}{\partial r} \qquad \overline{\Delta} = \frac{\partial \psi}{\partial \delta} \tag{A.2}$$

and the intrinsic dissipation expresses:

$$\dot{\Phi} = \underset{\sim}{\sigma} : \underset{\sim}{\dot{\varepsilon}^p} - \underset{\sim}{\mathbf{X}} : \underset{\sim}{\dot{\alpha}} - \overline{R}\dot{r} - \overline{\Delta}\dot{\delta} \tag{A.3}$$

The viscous stress $\sigma_v = f$ is given by Eq. (2) and the norm of the viscoplastic strain rate expresses by $\dot{p} = \dot{\lambda}$, taken from (4). The yield stress Y in (2) and the denominator K in (4) are assumed to write, like in (43):

$$Y = k + \overline{R} = k + (1 - \xi)R \qquad K = K_0 + \omega\overline{\Delta} = K_0 + \xi R \tag{A.4}$$

We choose a quadratic form of the stored energy potential, with:

$$\psi_p = \frac{1}{3} C \underset{\sim}{\alpha} : \underset{\sim}{\alpha} + \frac{1}{2}(1 - \xi) b Q r^2 + \frac{1}{2c}\xi Q^* \delta^2 \tag{A.5}$$

Parameters b and Q are those of the evolution equation of R in (39). Q^*, as well as ω in (A.4), will be shown later on. When applying (A.2) we find the associated thermodynamic forces as:

$$\underset{\sim}{\mathbf{X}} = \frac{2}{3} C \underset{\sim}{\alpha} \qquad \overline{R} = (1 - \xi) b Q r \qquad \overline{\Delta} = \frac{1}{c}\xi Q^* \delta \tag{A.6}$$

Let us choose the evolution equations for the three variables with the classical hardening – dynamic recovery format:

$$\underset{\sim}{\dot{\alpha}} = \underset{\sim}{\dot{\varepsilon}^p} - D \underset{\sim}{\alpha} \dot{p} \qquad \dot{r} = (1 - b r)\dot{p} \qquad \dot{\delta} = (c - b\delta)\dot{p} \tag{A.7}$$

C in (A.6-a) and D in (A.7-a) are the parameter of one back stress evolution in (5). From (A.7-b) and (A.7-c) it is easy to check that $\dot{\delta} = c\dot{r}$, so that (for 0 initial values) we obtain by integration $\delta = c\,r$. This is necessary in order to recover the restrictive case in which the same isotropic hardening R appears both in the yield stress Y and in the drag stress K, as we assumed in the present model. It results from (A.6-c) that:

$$\overline{\Delta} = \xi Q^* r = \frac{\xi Q^*}{bQ} R \tag{A.8}$$

Now, we may define the parameter ω in (A.4-b) in order to effectively have $\omega\overline{\Delta} = \xi R$. It writes:

$$\omega = b\frac{Q}{Q^*} \tag{A.9}$$

Using (A.6-a) in (A.7-a) we easily recover one of the back stress evolution equation (5), without a threshold in the dynamic recovery term and without the static recovery term. Static recovery is not considered in the present proof, as it is known to automatically induce a positive term in the dissipation. Similarly, using (A.6-b) in (A.7-b) we recover the evolution equation of one variable R. The mechanical part of the model is then completely recovered. Let us now check the dissipation. From (A.3) we get:

$$\dot{\Phi} = (\underset{\sim}{\sigma} - \underset{\sim}{\mathbf{X}}) : \underset{\sim}{\dot{\varepsilon}^p} - (\overline{R} + c\overline{\Delta}) + (D \underset{\sim}{\mathbf{X}} : \underset{\sim}{\alpha} + b\overline{R} r + b\overline{\Delta}\delta)\dot{p} \tag{A.10}$$

The direction of viscoplastic strain rate being given by (3), a simple calculation gives the first term as $J(\underset{\sim}{\sigma} - \underset{\sim}{\mathbf{X}})\dot{p}$. After rearrangement and taking into account (A.6-b) and (A.6-c) we easily get:

$$\dot{\Phi} = (J(\underset{\sim}{\sigma} - \underset{\sim}{\mathbf{X}}) - \overline{R} - k)\dot{p} + \left(k - c\overline{\Delta}\right)\dot{p} + \quad \frac{3D}{2C} \underset{\sim}{\mathbf{X}} : \underset{\sim}{\mathbf{X}} + (1 - \xi)\frac{R^2}{Q} + \xi\frac{c\,Q^*}{b\,Q}\frac{R^2}{Q}\Bigg)\dot{p} \tag{A.11}$$

As involving the viscous stress, the first term is always positive, from (2) and (A.4-a). The third one is obviously positive. The only term that could be negative is the second one. We now observe the role of the c parameter. As the mechanical response is totally independent of this parameter, it can be chosen freely, in order to be sufficiently small compared with the initial yield stress k. We always need a non-zero yield stress but it can be as small as we want. In practice it is sufficient to choose

$$c = \frac{k}{\mathrm{Max}(\overline{\Delta})} = \frac{b\,k}{\xi\,Q^*} \tag{A.12}$$

The last free parameter is Q^*. On the mechanical point of view it is totally free. However, it can be used to adjust the energy stored by the isotropic hardening, independently of the value of c. A last remark can be made, concerning the role of the additional state variable δ, associated with the isotropic hardening playing role in the drag stress K. If we eliminate the use of this additional variable, the dissipation will still be always positive but, in the particular case where $\xi = 1$ there will be no

stored energy associated with isotropic hardening. The use of this additional variable for the thermodynamic framework associated to the isotropic hardening in the drag stress, as well as the small parameter c, was considered first by Freed and Chaboche (1989).

References

Armstrong, P.J., Frederick, C.O., 1966. A mathematical representation of the multiaxial Bauschinger effect. Report RD/B/N731, CEGB, Central Electricity Generating Board, Berkeley, UK.

Belotteau, J., Berdin, C., Forest, S., Parrot, A., Prioul, C., 2009. Mechanical behavior and crack tip plasticity of strain aging sensitive steels. Materials Science and Engineering: A 526 (1–2), 156–165.

Benallal, A., Marquis, D., 1987. Constitutive equations for non-proportional cyclic elasto-viscoplasticity. Journal of Engineering Materials and Technology 109, 326–336.

Benallal, A., Berstad, T., Borvik, T., Hopperstad, O., Koutiri, I., Nogueira de Codes, R., 2008. An experimental and numerical investigation of AA5083 aluminium alloy in presence of the Portevin–Le Châtelier effect. International Journal of Plasticity 24 (10), 1916–1945.

Bóhlke, T., Bondár, G., Estrin, Y., Lebyodkin, M., 2009. Geometrically non-linear modeling of the Portevin–Le Châtelier effect. Computational Materials Science 44, 1076–1088.

Chaboche, J.L., 1989. Constitutive equations for cyclic plasticity and cyclic viscoplasticity. International Journal of Plasticity 5, 247–302.

Chaboche, J.L., 1996. Unified cyclic viscoplastic constitutive equations: development, capabilities and thermodynamic framework. In: Krauss, A.S., Krauss, K. (Eds.), Unified Constitutive Laws of Plastic Deformation. Academic Press Inc., pp. 1–68.

Chaboche, J.L., 1997. Thermodynamic formulation of constitutive equations and application to the viscoplasticity and viscoelasticity of metals and polymers. International Journal of Solids and Structures 34 (18), 2239–2254.

Chaboche, J.L., 2008. A review of some plasticity and viscoplasticity constitutive theories. International Journal of Plasticity 24 (10), 247–302.

Chaboche, J.L., Nouailhas, D., 1989. A unified constitutive model for cyclic viscoplasticity and its applications to various stainless steels. Journal of Engineering Materials and Technology 111, 424–430.

Chaboche, J.L., Dang-Van, K., Cordier, G., 1979. Modelization of the strain memory effect on the cyclic hardening of 316 stainless steel. In: SMIRT 5, Berlin.

Chaboche, J.L., Nouailhas, D., Pacou, D., Paulmier, P., 1991. Modeling of the cyclic response and ratcheting effects on Inconel 718 alloy. European Journal of Mechanics – A/Solids 10 (1), 101–121.

Chaboche, J.L., Kanouté, P., Azzouz, F., 2012a. Cyclic inelastic constitutive equations and their impact on the fatigue life predictions. International Journal of Plasticity 35, 44–66.

Chaboche, J.L., Kanouté, P., Gaubert, A., Azzouz, F., Lhachemi, D., Fournier, B., 2012b. Cyclic plasticity modelling of metallic materials exhibiting complicated rate dependent cyclic hardening or softening effects. In: Symposium Plasticity 2012.

Chen, L.J., Liaw, P.K., He, Y.H., Benson, M.L., Blust, J.W., Browning, P.F., Seeley, R.R., Klarstrom, D.L., 2001. Tensile hold low-cycle fatigue behavior of Cobalt-based Haynes 188 superalloy. Scripta Materialia 44, 859–865.

Chen, L.J., Liaw, P.K., He, H.W.Y.H., McDaniels, R.L., Jiang, L., Yang, B., Klarstrom, D.L., 2004. Cyclic deformation behavior of Haynes HR-120 superalloy under low-cycle fatigue loading. Mechanics of Materials 36, 85–98.

Dierke, H., Krawehl, F., Graff, S., Forest, S., Sach, J., Neuhäuser, H., 2007. Portevin–Le Châtelier effect in Al–Mg alloys: influence of obstacles – experiments and modelling. Computational Materials Science 39, 106–112.

El-Hefnawy, N.N., Abdel-Kader, M.S., Eleiche, A.M., 2012. Inclusion of DSA modeling capability in unified viscoplasticity theories, with application to Inconel 718 at 1100 °F. In: Krausz, A., Dickson, J.I., Immarigeon, J.-P.A., Wallace, W. (Eds.), Constitutive Laws of Plastic Deformation and Fracture. Kluwer Academic Publishers, pp. 67–73.

Estrin, Y., McCormick, P.G., 1991. Modelling the transient flow behaviour of dynamic strain ageing materials. Acta Metallurgica et Materialia 39 (12), 2977–2983.

Fournier, B., Sauzay, M., Caës, C., Mottot, M., Noblecourt, M., Pineau, A., 2006a. Analysis of the hysteresis loops of a martensitic steel – Part II: study of the influence of creep and stress relaxation holding times on cyclic behaviour. Materials Science and Engineering: A 437, 197–211.

Fournier, B., Sauzay, M., Caës, C., Noblecourt, M., Mottot, M., 2006b. Analysis of the hysteresis loops of a martensitic steel – Part I: study of the influence of strain amplitude and temperature under pure fatigue loadings using an enhanced stress partitioning method. Materials Science and Engineering: A 437, 183–196.

Fournier, B., Sauzay, M., Pineau, A., 2011. Micromechanical model of the high temperature cyclic behavior of 9–12%Cr martensitic steels. International Journal of Plasticity 27, 1803–1816.

Freed, A.D., Chaboche, J.L., 1989. Viscoplasticity: a thermodynamic formulation. NASA Tech. Memo. NASA TM-102388, NASA.

Freed, A.D., Walker, K., 1990. Model development in viscoplastic ratcheting. NASA Tech. Memo. NASA TM-102509, NASA.

Freed, A.D., Walker, K., 1993. Viscoplasticity with creep and plasticity bounds. International Journal of Plasticity 9, 213–242.

Graff, S., Forest, S., Strudel, J., Prioul, C., Pilvin, P., Bechade, J., 2004. Strain localization phenomena associated with static and dynamic strain ageing in notched specimens: experiments and finite element simulations. Materials Science and Engineering: A, 181–185.

Hähner, P., 1997. On the critical conditions of the Portevin–Le Châtelier effect. Acta Materialia 45, 3695–3707.

Ho, K., Krempl, E., 2001. The modeling of unusual rate sensitivities inside and outside the dynamic strain aging regime. Journal of Engineering Materials and Technology 123, 28–35.

Ho, K., Krempl, E., 2002. Extension of the viscoplasticity theory based on overstress (VBO) to capture non-standard rate dependence in solids. International Journal of Plasticity 18 (7), 851–872.

Krishna, S., Hassan, T., Ben Naceur, I., Saï, K., Cailletaud, G., 2009. Macro versus micro-scale constitutive models in simulating proportional and nonproportional cyclic and ratcheting responses of stainless steel 304. International Journal of Plasticity 25, 1910–1949.

Kubin, L.P., Estrin, Y., 1990. Evolution of dislocation densities and the critical conditions for the Portevin–Le Châtelier effect. Acta Metallurgica et Materialia 38, 697–708.

Lamba, H.S., Sidebottom, O.M., 1978. Cyclic plasticity for non-proportional paths. Journal of Engineering Materials and Technology 100, 96–111.

Lemaître, J., Chaboche, J.L., Benallal, A., Desmorat, R., 2009. Mécanique des Matériaux Solides,, Dunod, Paris.

Ling, C.P., McCormick, P.G., 1993. The effect of temperature on strain rate sensitivity in an Al–Mg–Si alloy. Acta Metallurgica et Materialia 41 (11), 3127–3131.

Mazière, M., Dierke, H., 2012. Investigations on the Portevin–Le Châtelier critical strain in an aluminium alloy. Computational Materials Science 52, 68–72.

Mazière, M., Besson, J., Forest, S., Tanguy, B., Chalons, H., Vogel, F., 2010. Numerical aspects in the finite element simulation of the Portevin–Le Châtelier effect. Computer Methods in Applied Mechanics and Engineering 199, 734–754.

McCormick, P.G., 1988. Theory of flow localization due to dynamic strain ageing. Acta Metallurgica 36 (12), 3061–3067.

Mesarovic, S.D., 1995. Dynamic strain aging and plastic instabilities. Journal of the Mechanics and Physics of Solids 43 (5), 671–700.

Miller, A., 1976. An inelastic constitutive model for monotonic, cyclic, and creep deformation: Part I. Equations development and analytical procedures. Journal of Engineering Materials and Technology 98 (2), 97–105.

Miner, R.V., Castelli, M.G., 1992. Hardening mechanisms in a dynamic strain aging alloy, hastelloy x; during isothermal and thermomechanical cyclic deformation. Metallurgical Transactions A 23A, 551–561.

Mühlhaus, H. (Ed.), 1995. Spatial Coupling and Propagative Plastic Instabilities. Wiley, pp. 395–450.

Nouailhas, D., Cailletaud, G., Marquis, D., Dufailly, J., Bollinger, E., Lieurade, H.P., Ribes, A., 1983. On the description of cyclic hardening and of initial cold-working. Engineering Fracture Mechanics 21 (4), 887–895.
Ohno, N., 1982. A constitutive model of cyclic plasticity with a non-hardening strain region. Journal of Applied Mechanics 49, 721.
Ohno, N., Wang, J.D., 1993. Kinematic hardening rules with critical state of dynamic recovery, Parts I and II. International Journal of Plasticity 9, 375–403.
Portevin, A., Le Châtelier, M., 1923. Tensile tests of alloys undergoing transformation. Comptes Rendus de l'Académie des Sciences Paris 176, 507.
Rao, R.B.S., Castelli, M.G., Ellis, J.R., 1995. On the low-cycle fatigue deformation of Haynes 188 superalloy in the dynamic strain aging regime. Scripta Metallurgica et Materialia 33 (6), 1005–1012.
Rao, R.B.S., Castelli, M.G., Allen, G.P., Ellis, J.R., 1997. A mechanical assessment of the mechanistic aspects in Haynes 188 during low-cycle fatigue in the range 25 °C to 1000 °C. Metallurgical and Materials Transactions A 28A (6), 347–361.
Schmidt, C.G., Miller, A., 1981. A unified phenomenological model for non elastic deformation of type 316 stainless steel. Parts I and II. Res Mechanica 3, 109–129, 175–193.
Tanaka, E., Murakami, S., Ooka, M., 1987. Effects of strain path shapes on non-proportional cyclic plasticity. Journal of the Mechanics and Physics of Solids 33, 559–575.
Van den Beukel, A., 1975. Theory of the effect of dynamic strain aging on mechanical properties. Physica Status Solidi 30, 197–206.
Yaguchi, M., Takahashi, Y., 2000. A viscoplastic constitutive model incorporating dynamic strain aging effect during cyclic deformation conditions. International Journal of Plasticity 16, 241–262.
Yaguchi, M., Yamamoto, M., Ogata, T., 2002. A viscoplastic constitutive model for nickel-base superalloy. Part I: kinematic hardening rule of anisotropic dynamic recovery. International Journal of Plasticity 18, 1083–1109.
Yao, D., Krempl, E., 1985. Viscoplasticity theory based on overstress. The prediction of monotonic and cyclic proportional and nonproportional loading paths of an aluminium alloy. International Journal of Plasticity 1, 259–274.
Zaizer, M., Hähner, P., 1997. Oscillatory modes of plastic deformation: theoretical concepts. Physica Status Solidi B 199, 267–330.
Zebulon, 2011. Z-SET/ZéBuLoN, material and structure analysis suite. <http://www.zset-software.com/>.
Zhang, S., McCormick, P.G., Estrin, Y., 2001. The morphology of Portevin–Le Châtelier bands: finite element simulation for Al–Mg–Si. Acta Materialia 49, 1087–1094.